JOURNAL OF MATERIALS SCIENCE 20 (1985) 3385 – 3399

Formability of sheet metal with heterogeneous damage

F. BARLAT, J. M. JALINIER
Genie Physique et Mecanique des Materiaux – UA CNRS 793, Institut National Polytechnique de Grenoble, BP 46, 38402 Saint Martin D'Heres Cedex, France

During sheet metal forming operations, internal damage occurs as a result of nucleation, growth and coalescence of cavities around particles, inclusions or second phase. In this work, this phenomenon is experimentally studied by relative density change measurements and scanning electron microscope observations in a dual-phase steel sheet. It is observed that the distribution of cavities is not homogeneous. A model of plastic flow localization is proposed taking account of a non-uniform void distribution. The results show a substantial reduction in the formability of the sheet as well as anisotropic effects due to the heterogeneous distribution of voids.

1. Introduction

The formability of a sheet metal is directly related to its ability to plastically deform. The material parameters controlling the plastic deformation can be considered on two levels: (a) a macroscale, where constitutive parameters are derived from the overall material behaviour such as strain-hardening, strain rate hardening and plastic anisotropy; and (b) a microscale, where structural parameters are physically determined from an understanding of the different mechanisms involved in a plastic deformation: roughness, grain size, texture, dislocations microstructure, inclusions content, internal damage etc.

Although it is obvious that these two classes of parameters are strongly related, the relationships between them are not yet clear. Our approach, as usually done, separates the influence of each parameter. The plastic behaviour of the material and more precisely the onset of plastic instability will be described by the constitutive parameters, and only one structural parameter will be considered: internal damage.

2. Internal damage

2.1. Method of analysis

In sheet metal forming, the industrial materials usually present a high content of particles: inclusions, precipitates and second phases. Plastic deformation will generally induce void nucleation around the particles during any forming process including cold rolling, deep-drawing and stretch forming. Therefore only volumic internal damage related to particles will be taken into account; the analysis will not be valid for planar defects such as fatigue cracks, which are not observed in the forming processes considered. Two main damage mechanisms have been observed [1]: (a) by decohesion of the particle–matrix interface (mainly for equiaxed particles); and (b) by failure of the particle (mainly for elongated particles).

In commercial materials, this classification into two mechanisms may not be obvious as particles can break and give decohesion at the same time, or two different mechanisms can be observed on two classes of particles of different morphology.

One effect of the internal damage is to reduce the plastic formability by accelerating the plastic instability process. This phenomenon will then lead to ductile fracture by excessive growth and coalescence of the cavities.

2.2. Measurements

Different experimental phenomena have been proposed and used to quantify the internal

0022–2461/85 $03.00 + .12

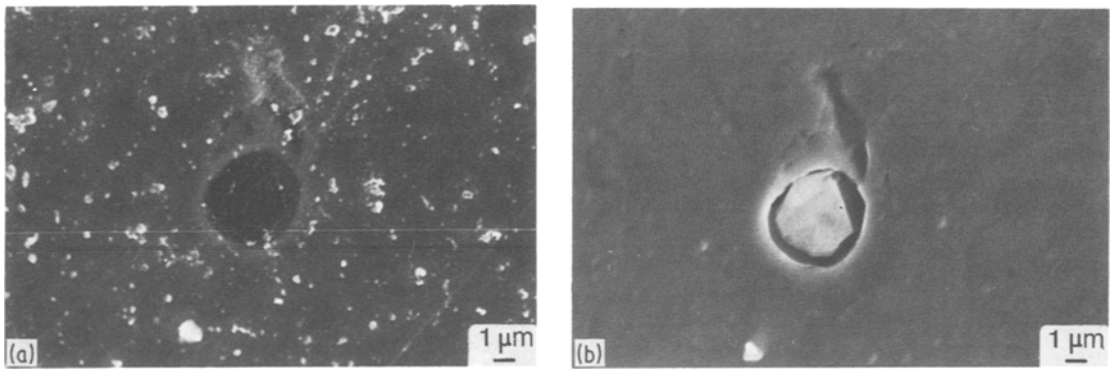

Figure 1 Damage by decohesion between the matrix and an alumina particle in a dual-phase steel sheet: (a) before ion-polishing, (b) after ion polishing.

damage: Young's modulus changes [2], acoustic emission, hydrogen diffusion, X-ray or neutron diffraction. In this work we have used two other complementary techniques: relative density change measurements, and microscopic observations. The relative density change measurements are carried out using the Ratcliffe technique [3] which consists in weighing a deformed and a reference sample alternatively in the air and in a liquid. The accuracy of this measure is of the order of $\pm 5 \times 10^{-5}$. The metallurgical observations are carried out using a scanning electron microscope. The samples are prepared by mechanical and subsequent ion polishing [4, 5]. This technique is necessary to obtain reliable observations as shown in Fig. 1.

The density method gives an accurate value of the volumic growth of the cavities. This accuracy is obtained by relative measurements which do not allow one to determine the absolute value of the reference sample, for example the initial damage for a reference undeformed sample. Furthermore, no information is obtained on the physical aspect of damage. Conversely, the microscopical observations give physical details: damage mechanism; shape, size and distribution of the cavities; chemical nature of the particles responsible for void formation. Accuracy is very difficult to achieve on these observations as it statistically requires a significant number of measurements. Furthermore, for complex void shapes the transfer from surface observation to volumic parameters is not easy if not impossible.

The combination of these two techniques is powerful: it gives complementary parameters in perfect agreement [6]. Since it can be shown from the stereological laws [7] that $C_v = C_s$ where C_v is the void volume fraction and C_s the surface fraction of voids intercepted by a section, the following relationship can be drawn [8]:

$$-\frac{\Delta d}{d} = C_v - C_{v0} = C_s - C_{s0} \quad (1)$$

where $-\Delta d/d$ is the relative density change between a deformed and a reference sample (subscript 0).

As an example of the use of these two methods, the relative density change for different materials deformed in uniaxial tension (austenitic stainless steel) and equibiaxial stretching (all others) is presented on Fig. 2. A monotonic decrease of the relative density is observed, and this decrease is confirmed by the microscopical observations which reveal a regular distribution of cavities. Figs. 3a and b show a typical evolution of the number and size of cavities in the austenitic steel considered. A simple estimation of the surface fraction of voids in case of Fig. 3b gives an estimation of the density change in very good agreement with the measurements, using Equation 1.

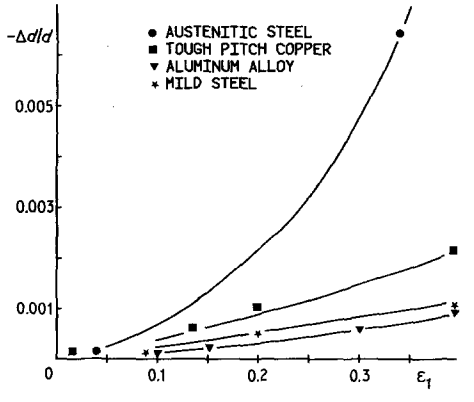

Figure 2 Relative density change against principal strain for several materials.

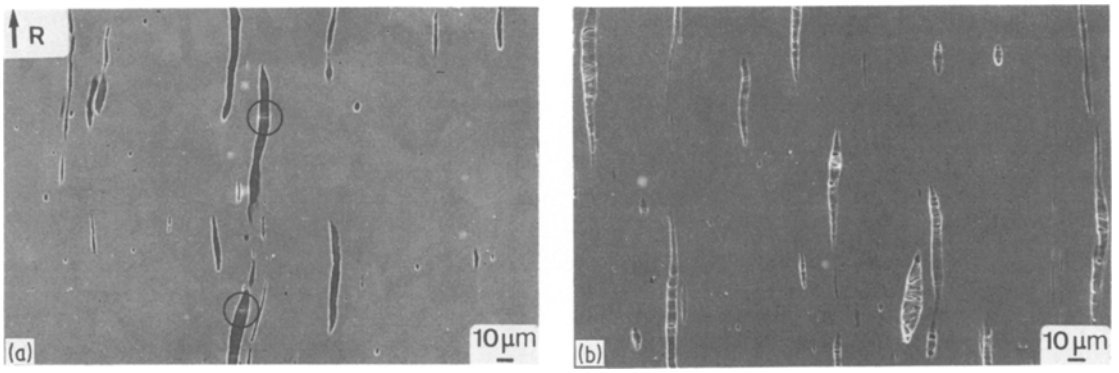

Figure 3 Failure of MnS particles in an austenitic stainless steel after uniaxial straining (R is the rolling direction): (a) $\varepsilon_1 = 0.04$, (b) $\varepsilon_1 = 0.34$.

2.3. Application to the case of a dual-phase steel

The case of a dual-phase steel has been extensively studied for different linear strain paths ϱ (minor to major incremental principal strain in the plane of the sheet): (a) uniaxial tension ($\varrho = d\varepsilon_2/d\varepsilon_1 = -0.5$); (b) plane strain ($\varrho = 0$); and (c) equibiaxial stretching ($\varrho = 1$).

The chemical analysis as well as the mechanical properties of this material are listed in Tables I and II. The relative density changes measured are shown in Fig. 4 (together with surface microscopical measurements for equibiaxial stretching). A great discrepancy between the results can be observed and no evolution of the damage can be derived. Furthermore, measurements on two different samples at the same deformation level give two different values (Points A and B, C and D). The question of the homogeneity of the material on the scale of the measurements arises. These heterogeneities in the damage distribution are confirmed by density measurements of two neighbouring samples ($1 \times 4\,cm^2$) which gives a value of $-\Delta d/d = 1.5 \times 10^{-3}$. It has to be noticed that this value is of the same order as the one involved in void growth. Therefore, no conclusion on the damage evolution can be drawn from the density measurements. Microscopical observations reveal the existence of a distribution in size of the cavities. The heterogeneities appear to be due to a non-uniform distribution of the biggest cavities.

TABLE I Chemical analysis of the dual-phase steel

Element	C	Mn	Cr	P	S	N	Al	Si
Content (10^{-3} %)	36	1105	573	11	10	5	39	32

3. Analysis of the heterogeneities in the dual-phase steel

3.1. Physical aspect of the damage

The microscopical observations carried out for a large number of sites show important differences in the volume fraction of voids at the scale of a few centimetres. In these different places, the size of the cavities is the same, only their number is different (Fig. 5). These cavities can be divided into three groups according to the nature of the particle at the origin of the void:

(a) Very small cavities associated with manganese sulphide inclusions (Fig. 6). On this figure N denotes the direction normal to the plane of the sheet.

(b) Big cavities associated with alumina particles (Fig. 7).

(c) Associated with second phase particles, only rare cavities can be found even for relatively large deformations ($\varrho = 1$, $\varepsilon_3 = -0.57$). According to different authors [9–12] it seems that decohesion around second-phase particles happens only at large plastic strain, often

TABLE II Mechanical properties of the dual-phase steel sheet

Yield strength (0.2%) σ_y (MPa)	Tensile strength σ_t (MPa)	Total elongation to fracture A (%)	Mean anisotropic strain ratio (width to thickness strain) $\bar{r}$
219	453	32.8	1.01

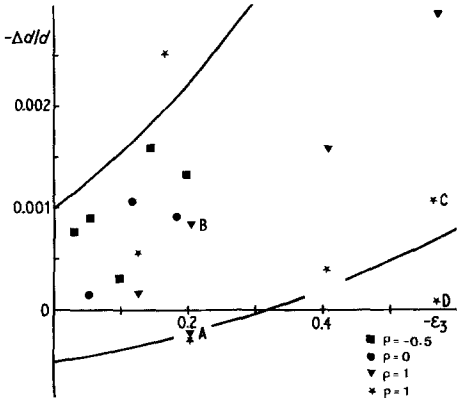

Figure 4 Relative density change as a function of the thickness strain ε_3 for a dual-phase steel sheet strained under different strain paths.

post-necking. As an example, Fig. 8 shows a nital-etched sample where the void in the centre is due to an alumina particle as in Fig. 7, but no cavity appears around the second phase (small light island).

3.2. Statistical analysis of the damage

Quantitative microscopical observations are performed in order to assess the evolution of damage during plastic deformation for equibiaxial stretching. In order to characterize the cavities several parameters are measured, in particular the number per unit area and the surface fraction of voids. As has been shown for other materials [13, 14], initial damage due to rolling is present in the dual-phase steel before any plastic deformation. For all the strained specimens, there are found small cavities (Fig. 9a) and large cavities (Fig. 9c). This leads us to classify the areal section, S, of cavities in three classes (Table III): (a) $S < 3\,\mu m^2$; (b) $3\,\mu m^2 < S < 15\,\mu m^2$; and (c) $15\,\mu m^2 < S$.

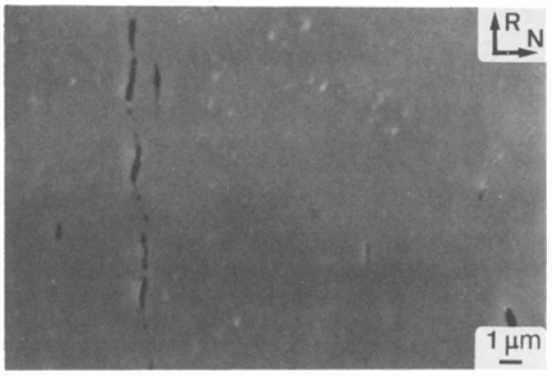

Figure 6 MnS inclusions in the dual-phase steel ($\varrho = -1/2$, $\varepsilon_3 = -0.05$): R is the rolling direction.

As mentioned before, the distribution of these cavities is not uniform. The material considered exhibits two types of heterogeneity that clearly appear when examining the two neighbouring samples having a relative density difference of 1.5×10^{-3}. In the first type the material can be divided into areas of approximately $4\,cm^2$ (sample size for density measurements) in which the distribution of voids is roughly uniform, but where the number of cavities per unit volume varies from one area to another. The second type shows the presence of bands with a high fraction of cavities, parallel to the plane of the sheet and aligned in the rolling direction. The width of these bands is $150\,\mu m$ and the length can reach 20 mm. Fig. 5 is a part of this type of heterogeneity.

Owing to the heterogeneous nature of the damage, care must be taken with the statistical measurements. In particular, no evolution can

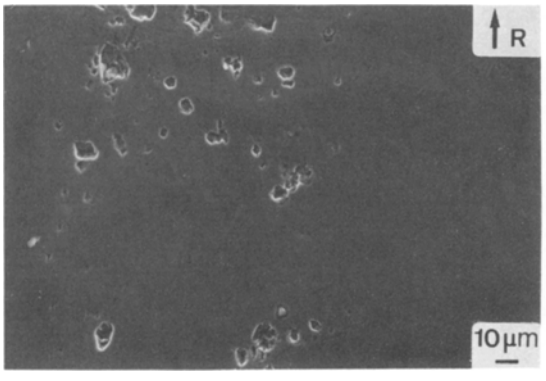

Figure 5 Heterogeneous void distribution in the dual-phase steel ($\varrho = -1/2$, $\varepsilon_3 = -0.03$); R is the rolling direction and N the normal direction (transverse).

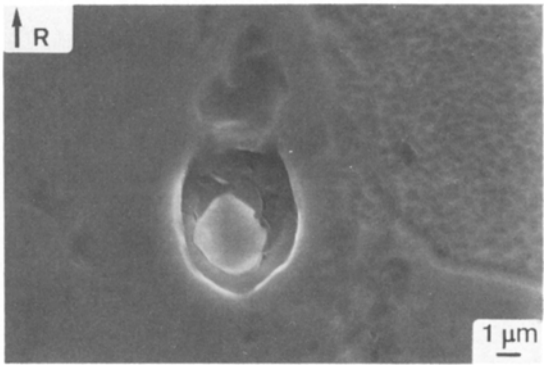

Figure 7 Decohesion of the matrix around an alumina particle in the dual-phase steel ($\varrho = -1/2$, $\varepsilon_3 = -0.07$); R is the rolling direction.

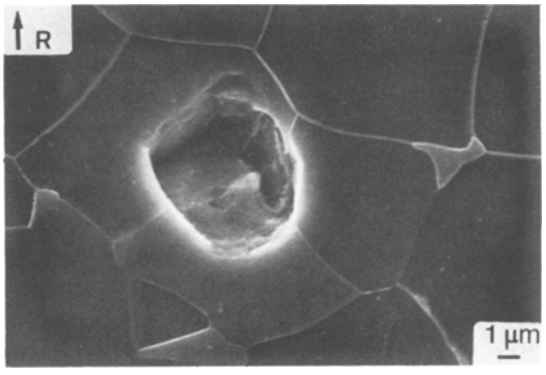

Figure 8 Cavity and second phase particles in the dual-phase steel ($\varrho = -1/2$, $\varepsilon_3 = -0.07$); R is the rolling direction.

be deduced from the void parameters. For instance, the observations performed on two different samples at the same deformation stage ($\varrho = 1$, $\varepsilon_1 = 0.285$) give conflicting results. Nevertheless, it would not be consistent to perform experiments at a larger scale. In fact, the scale of necking corresponds to the scale of the damage heterogeneities, and thus it is of major importance to account for this phenomenon. The purpose of the following sections is to characterize the cavities and their distribution in the material.

3.3. Size of the cavities

In order to simplify, it is assumed that the material contains only one or two classes of initially spherical cavities. An explanation can be given for the presence and the heterogeneous distribution of the small sections ($S < 3\,\mu m^2$). Fig. 6 shows manganese sulphide inclusions in a plane normal to the plane of the sheet. If a metallographic plane parallel to the plane of the sheet intersects these inclusions, it would give small sections as in Fig. 9a, aligned in the rolling direction. In fact, the effect of the small cavities will be neglected since a part of them can be the result of the mechanical polishing. Moreover, it has been shown that sheet formability is rather affected by the big cavities [15].

Finally, from the results in Table III, it is inferred that two classes of cavity are required in order to represent the material. A simple statistical calculation carried out on the undeformed sample allows one to size the cavities: Class A with initial radius $R_{A_0} = 4.2\,\mu m$, and Class B with initial radius $R_{B_0} = 2\,\mu m$.

3.4. Growth of the cavities

During plastic deformation the density of the material decreases by nucleation and growth of voids. In this model, all cavities are supposed to be present before any plastic deformation. This assumption is based on the experimental evidence of initial damage. Furthermore, among numerous nucleation criteria [16–24] it seems that large inclusions like alumina in the dual-phase steel produce cavities in the first stage of

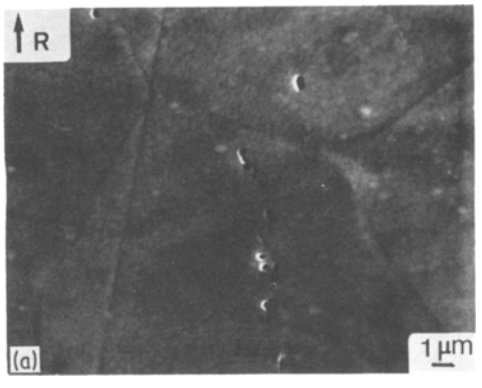

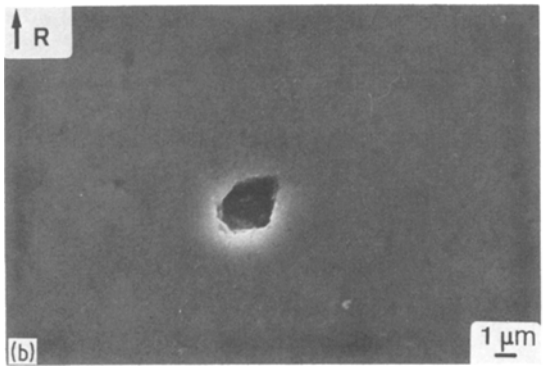

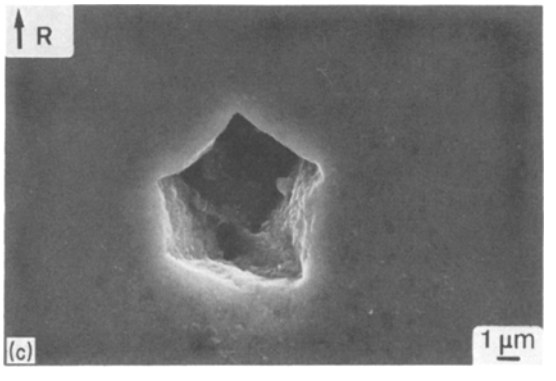

Figure 9 Cavities of different sizes in the dual-phase steel: (a) small size ($\varrho = 1$, $\varepsilon_3 = -0.06$); (b) medium size ($\varrho = -1/2$, $\varepsilon_3 = -0.03$); (c) large size ($\varrho = -1/2$, $\varepsilon_3 = -0.03$). R is the rolling direction.

TABLE III Statistical parameters of voids measured in the dual-phase steel at different levels of strain ε_1 in equibiaxial stretching

Range of sections (μm^2)	Parameter measured	ε_1					
		0	0.063	0.102	0.204	0.285	0.285
< 3	N_a (mm^{-2})*	292	1425	446	506	35	1187
	S (μm^2)†	0.31	0.29	0.18	0.24	0.73	0.27
3 to 15	N_a (mm^{-2})	15.5	75	13.5	12.5	16	12.5
	S (μm^2)	8.2	6.1	6.4	4.1	7.9	9.4
> 15	N_a (mm^{-2})	4	–	–	19	26	–
	S (μm^2)	41.6	–	–	30.4	47.8	–

*Number of sections per unit area.
†Mean of the sections.

the straining. So, the further development will only deal with the growth of cavities.

Rice and Tracey [25] have studied the growth of a spherical void in a non-hardening plastic matrix. The equations that they have obtained have been linearized for simple [8] and complex [15] strain paths and can be written

$$dR_i/R_i = C d\varepsilon_i - K d\varepsilon_3 \quad (2)$$

where R_i and ε_i are respectively the radius of the void and the plastic deformation imposed to the sheet in the i direction, C and K two constants equal to 5/3 and 0.64. $C d\varepsilon_i$ is a deviatoric term associated with a change in shape at constant volume, and $K d\varepsilon_3$ a spherical term associated with homothetic change in volume. This equation is assumed to be valid for hardening material, which seems to be correct considering the low stress triaxiality in the sheet [26]. Moreover, the interaction between the cavities is neglected. The damage growth can be expressed [15] by

$$C_v = C_{v0} \exp(-3K\varepsilon_3) \quad (3)$$

where C_v and C_{v0} are the void volume fractions in the strained and reference material.

In order to verify the validity of the model, quantitative metallographic observations are simulated. In particular, the mean intercepted void section for sections larger than 15 μm^2 is calculated as a function of the thickness strain (Fig. 10). These curves explain why the experimental mean (Table III) first decreases (ε_1 = 0.204) and then increases.

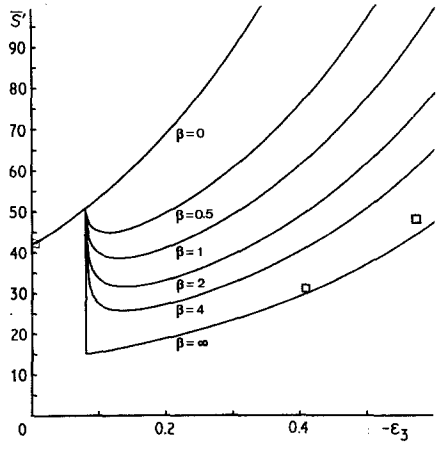

Figure 10 Theoretical evolution of the mean of void sections larger than 15 μm^2 observed in a plane as a function of the thickness strain. β is the ratio of the volume number of voids (n_B/n_A). R_{A_0} and R_{B_0}, the initial radii of the spherical cavities, are 4.2 and 2.0 μm respectively. The squares are experimental points.

3.5. Distribution of the cavities

As has been mentioned before, the studied dual-phase sheet can be divided into areas of about 4 cm^2 in which the distribution of voids differs from one area to another. Moreover, some bands are observed with a high fraction of cavities. However, it has to be noticed that the presence of such alignments of cavities does not affect the volume fraction of voids in a 4 cm^2 sheet which is the size required for the density measurements. Among twelve neighbouring samples deformed in uniaxial tension (ε_3 = −0.03) the maximum difference between two samples is 1.5×10^{-3}. A quantitative metallographic study performed on these two samples allows one to find the corresponding surface fraction of voids: 2.3×10^{-3} and 9×10^{-4}. These values seem to be in perfect agreement by using Equation 1. Nevertheless, this equation is not valid for the case of heterogeneous damage.

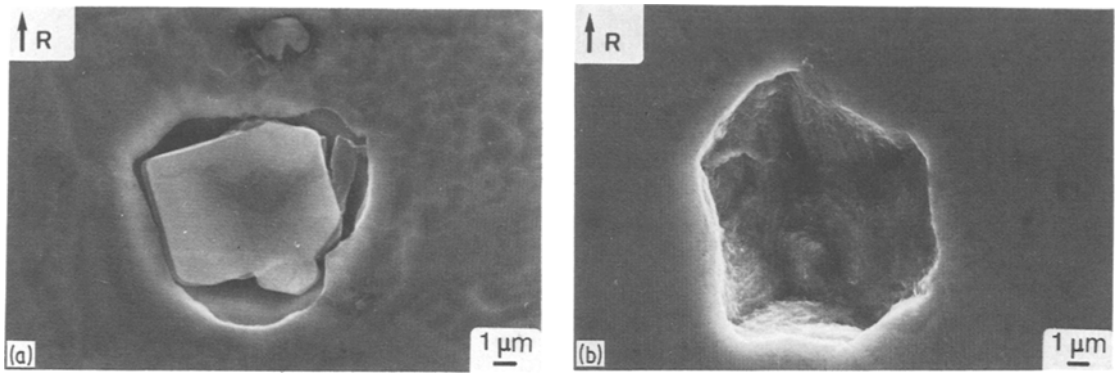

Figure 11 Decohesion of the matrix around alumina particles in the dual-phase steel ($\varrho = -1/2$, $\varepsilon_3 = -0.07$): (a) ion polishing, (b) nital etching, then slight mechanical polishing (the particle has disappeared). R is the rolling direction.

Fig. 11 shows typical cavities in the dual-phase steel with or without an inclusion inside. In fact, in Fig. 11b the inclusion has disappeared during polishing. Two absolute values of damage measurements can be given by either taking away the surface fraction of the inclusion or not. However, in the two cases and for homogeneous materials the relative change will give the same result with the use of Equation 1 provided that all measurements are consistent. In contrast, for heterogeneous materials the relative density difference is due on the one hand to the inclusion content, which differs from one sample to another even at the same deformation stage, and on the other hand to the cavities associated with the inclusion. So, the relative density change measurements for a heterogeneous material take account of these two phenomena. Thus, a more accurate description of the density change is derived from a model that assumes that the material contains spherical inclusions of radius R_{in} inside cavities of radius R_{ca}, where $R_{in}/R_{ca} = \delta$. It is assumed that the linearized equations for the growth of voids are valid. Before any plastic deformation the relative density change between two samples is

$$-\frac{\Delta d}{d} = (C'_{v_0} - C_{v_0})(1 - k\delta^3)$$

where k is the density ratio of the inclusion and the matrix (ϱ_i/ϱ_m) and C_v the void volume fraction (including inclusions) for the two specimens 0′ and 0. The use of the damage growth laws allows one to obtain the relative density change between a strained (subscript 1) and a reference (subscript 0) sample:

$$-\frac{\Delta d}{d} = C_{v_1}[\exp(-1.92\varepsilon_3) - k\delta^3] - C_{v_0}(1 - k\delta^3) \quad (4)$$

A system of three equations with four unknowns can be drawn from Equation 4 by taking the relative density change from Fig. 4 (full lines) and by using the relative density difference of 1.5×10^{-3} for the two neighbouring samples. The unknowns are $C_{v_{max}}$, $C_{v_{min}}$ (the extremal void volume fractions), C_{v_0} (the void volume fraction of the reference sample for all the measurements of Fig. 4) and δ ($= R_{in}/R_{ca}$). With the estimations provided by the quantitative metallographic observations, the best compromise to solve the system gives

$$C_{v_{max}} = 2.6 \times 10^{-3} \quad C_{v_{min}} = 0.6 \times 10^{-3}$$
$$C_{v_0} = 1.3 \times 10^{-3} \quad \delta = 0.8$$

The δ value leads to a ratio C_{sc}/C_{si} of the surface fraction of voids to the surface fraction of inclusions in the as-received material equal to 0.5, which is comparable with the experimental ratio of 0.2 measured in tough pitch copper [27]. Subsequently, the minimal and maximal values of initial void volume fraction will be taken as 0.6×10^{-3} and 2.6×10^{-3}.

4. Prediction of the forming limit diagram for isotropic material with volume damage

Though volume damage is often analysed as a factor leading to ductile failure, it also has an effect leading to unstable plastic flow from the earliest deformation stages. This underscores its

importance with respect to plastic instability phenomena. So, emphasis is given to the influence of damage on the forming limit diagram, which represents the relationship between limiting major and minor principal strains of the plane of the sheet just before sharp necking.

4.1. Different ways to introduce damage in plastic instability calculations

Chu [28] analysed different factors giving rise to high deformation gradients during the stamping of an axially symmetric sheet using a circular die. A finite element method was used to examine the effects of friction and boundary conditions. Volume damage was introduced through Gurson's plastic flow criterion for porous material [29] as well as the flow laws associated with this criterion. Chu showed that the presence of cavities reduces the formability of the material. However, in order to have reasonable results, she had to introduce initial void volume fraction values of 0.01 to 0.03, and these evolve to values of 5 to 10% for stages just preceding the necking. It seems that these values are much too high as compared with those usually measured for sheet metal [39], namely 10^{-3} to 5×10^{-3}.

The model of Marciniak and Kuczynski (M–K) uses a macroscopic description of the material [31, 32]. This assumes that after a certain amount of deformation, flow becomes localized on a defect represented by a narrow linear band initially present in the material (Fig. 12). One supposes that the material has properties in this band different from those in the homogeneous portion, and this difference is modelled by a smaller thickness or section area at the band that involves a defect D defined by

$$F = 1 - D = t_a^0/t_b^0$$

where ⟨a⟩ and ⟨b⟩ are the zones marked in Fig. 12. Equilibrium equations show that the stress is

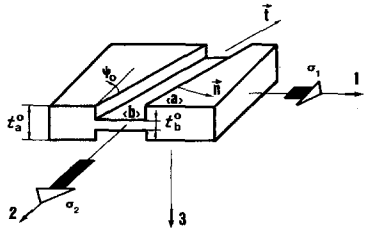

Figure 12 Model of localized necking in the Marciniak–Kuczynski analysis.

higher in Zone ⟨b⟩, and hence plastic flows in the two zones differ from each other.

For the basic Marciniak model, Needleman and Triantafyllidis [23] have shown that one can consider the following defect types: thickness heterogeneity between the homogeneous portion and the defect, work-hardening heterogeneity, and different flow stresses. They also studied the heterogeneity due to a greater volume fraction of cavities near the defect. The constitutive equations for porous material of Gurson [29] were introduced. To obtain theoretical forming limit curves in agreement with experimental results, they had to use initial volume fraction values of the order of 10^{-2}. As in the study of Chu [28], these appear to be unreasonably high. Nevertheless, the authors have concluded that the different shapes in the forming limit curves may be attributed to the growth of cavities.

Furthermore, Chu and Needleman [34] have analysed the influence of cavity nucleation on the forming limit calculated as in the previous investigation. Various nucleation criteria were introduced in the equations, and in particular a criterion based on a critical equivalent strain. It was assumed that cavities appear at strains normally distributed around the critical strain. It was shown that when the standard deviation of this normal law is small (almost all of the cavities appear at the same strain), all the cavities are created in the defect and not in the less deformed homogeneous portion. This explains why the influence of nucleation in this case is very destabilizing and leads to rather low forming limit curves.

Melander and co-workers have developed a theory [9, 27, 35] in which the geometrical model is identical to the M–K model. Melander supposed, however, that the heterogeneity is a region of the material where the volume fraction of inclusions is greater than the mean value. It is a region whose thickness is not necessarily different from that of the homogeneous portion. He assumed the volume fraction of cavities to be a function of that of inclusions and of the accumulated strain in each of the two regions of the material. This function may be identified by quantitative microscopy. As in the previous studies, he introduced the volume fraction of cavities in the equations of his model using Gurson's criterion. For numerical applications, he

used experimental values of strain-hardening, strain rate sensitivity, anisotropy (r) and mean initial inclusion concentration. The only unknown is the inclusion concentration in the defect. He used this as a fitting parameter for the agreement of theoretical and experimental curves. This led him to conclude that the purer the material, the more concentrated must the inclusions be in the defect in order for the theory to be satisfactorily applicable to different materials.

Damage was introduced in a different manner by Jalinier and Schmitt [8, 36]. They considered that the volume dilatation is negligible and that the constitutive laws of incompressible plasticity are valid. Damage was introduced through a statistical study in which it was shown that plane sections in the material intersect a great number of cavities. These sections will then have a smaller area than the average section. This section defect is then assumed to be equivalent to a thickness defect which enables them to identify the model to be that of Marciniak. However, they have added to the defect increase due to heterogeneous plastic flow, a defect increase due to cavity growth. Through this method, physical parameters based on quantitative microscopic observations can be introduced. The forming limit curves obtained are in good agreement with experimental curves. Furthermore, their theory has explained why thinner sheets give rise to less satisfactory deformation, and this is a well-known experimental observation.

A purely statistical method has been proposed by Van Minh, Sowerby and Duncan [37, 38] to explain the distribution of experimentally observed deformation limits for a given material and a given operation. This study is based on the hypothesis that Marciniak's theory holds for an elementary surface of a sheet in which a certain cavity distribution exists. The defect amplitude is given by the largest cavity in this element. After a probability calculation, it is possible to associate with a given stamping operation a forming limit obeying a statistical distribution law. The authors have shown that the mean deformation limit decreases as the cavity mean size increases, or as the sheet thickness decreases. However, this statistical investigation introduces very arbitrary parameters to describe cavities.

4.2. Model used in this work

As for the work of Jalinier and Schmitt [8, 36], the plastic instability M–K model [31, 32] for isostropic materials, extended for the complex strain paths by Barata de Rocha and Jalinier [39], is chosen as a basic model. A physical explanation of the section defect can be given from the concept of damage. For a given distribution of cavities there exist sections, normal to the sheet plane, which intercept more cavities than other sections. For a random distribution of cavities in a material, a statistical study shows the existence of these sections.

This determination, developed elsewhere [15, 40], is divided into two parts:

(a) The first consists of calculation for a point on the sheet the probability of finding a local defect, due to the superimposition of one or several cavities, along a line passing through the point and normal to the sheet plane (Fig. 13). This calculation has been already done for the cases of one class of cavities or of two classes of cavities [8].

(b) The second considers a local defect distribution and calculates a linear defect F equivalent to the defect of the plastic instability model used in the M–K theory (Fig. 14) by obtaining the mean of all local defects which belong to an approximately linear band.

The final expression of the defect factor F for two classes of cavities (Appendix A) is:

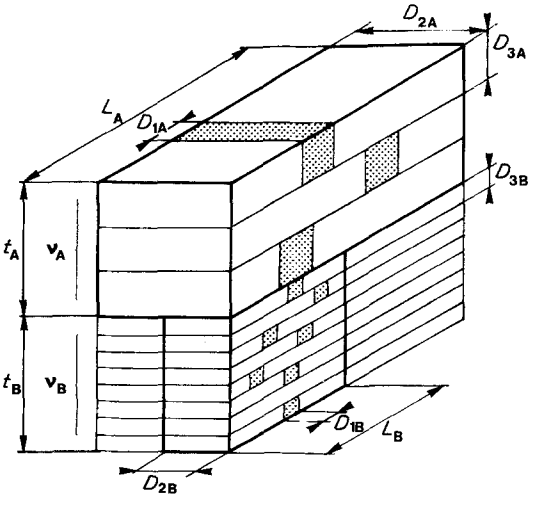

Figure 13 Model of the thickness of a material containing two classes of voids (from [8]).

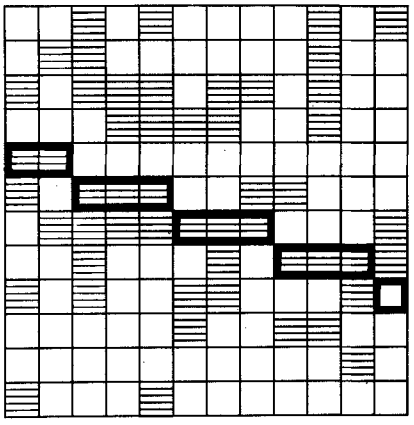

Figure 14 Model of the plane of the sheet. Shaded areas correspond to a local defect due to the superimposition of one or more cavities. A quasi-linear band joining a maximum number of local defects is represented. This band is a weak section of the sheet where localized plastic flow could appear.

$$F = \left[1 - \frac{C_v}{1 - (1 - C_v)^{v_A + v_B}}\right] p^h + 1 - p^h \tag{5}$$

where C_v is the total void volume fraction, p^h the probability of finding a defect in a narrow quasi-linear band joining a maximum local defect. v_A and v_B characterize the size of the cavities:

$$v_A = \frac{(C_{vA}/C_v)}{(t_0/R_{A_0})}$$

$$v_B = \frac{(C_{vB}/C_v)}{(t_0/R_{B_0})}$$

where C_{vA} and C_{vB} are the void volume fraction of Class A and Class B, R_{A_0} and R_{B_0} the initial void radius and t_0 the initial sheet thickness. The determination of the F value obtained in this work is different from the value determined by Jalinier and Schmitt [36]. In their analysis, the defect that they took into account in calculations corresponded to the local defect which interacts with other defects of the same amplitude. However, this analysis is not valid for the case of the big cavities that can be found in the dual-phase steel, since only one cavity gives much too low an F value; it is impossible to find a point defect and the associated probability of existence in order to optimize the interaction condition.

Using the damage growth law (Equation 3), the initial defect and its evolution can be computed. Fig. 15 shows how the defect increases for various conditions. Since this type of defect is determined by a statistical calculation it will be called a statistical defect. It is worthy of note that the statistical defect can develop for any homogeneous damaged material and in any direction of the sheet.

In the present study, it has been seen that the dual-phase steel sheet can be divided into areas of about 4 cm^2 in which the void volume fraction is constant. Hence, the above analysis of statistical defects can be applied in each of these areas, and obviously the plastic flow localization will occur in the area which contains the larger

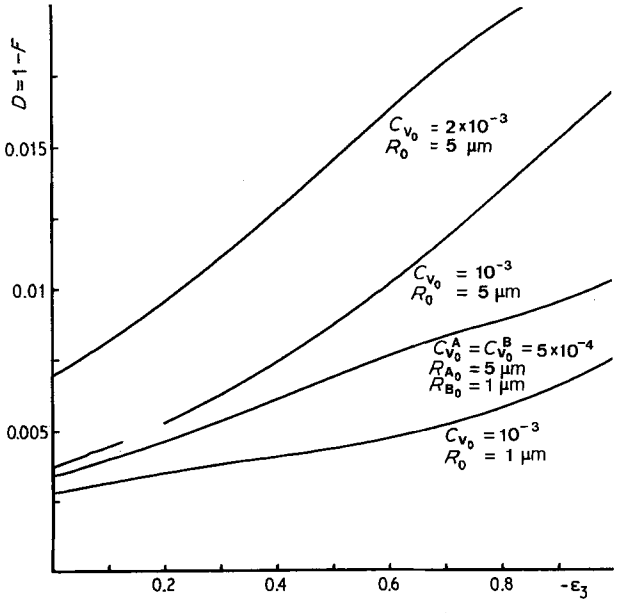

Figure 15 Evolution of the statistical defect with the thickness strain for different types of damage conditions; t = 0.7 mm.

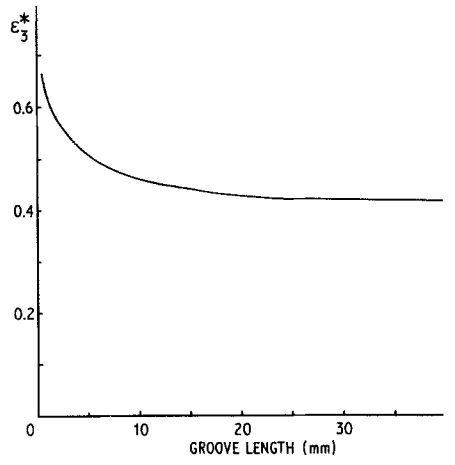

Figure 16 Influence of the groove length on the thickness limit strain for an aluminum alloy (from [41]).

defect. The important thing is to notice that the scale of these areas is large enough to produce a plastic instability. In fact, it can be related to experimental work [41] which has consisted in making grooves of different lengths but of constant F value in an aluminium sheet. The influence of the groove length on the limit thickness strain before flow localization is reproduced in Fig. 16. From this curve, the authors have concluded that continuous weak regions which are larger than about $10t_0$ can behave like M–K grooves.

The statistical defect is not the only one that can be found in dual-phase steel. The cavity bands observed in this material are at the origin of defects. Since these defects develop only in the rolling direction they are called structural defects. They can be modelled as shown in Fig. 17. The amount and the evolution of the structural F value is calculated taking account of the direction of the band (rolling) according to the principal axes (ψ) and the growth of cavities (Appendix B):

$$F = F(R_{A_0}, R_{B_0}, l_0, t_0, \varrho, \varepsilon_1, \psi) \quad (6)$$

Neglecting the stress concentration in such cavity bands it can be shown, using a simple criterion of critical spacing between voids [42, 43] that coalescence in the overall band cannot be reached before necking. Moreover, the length of the band (10 to 20 mm) is large enough so that the sheet behaves like an M–K material.

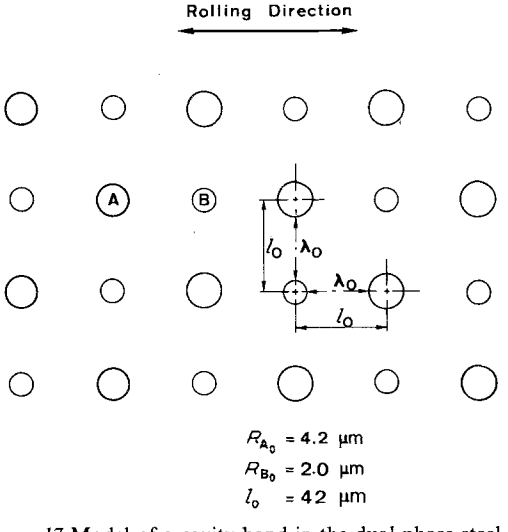

Figure 17 Model of a cavity band in the dual-phase steel.

4.3. Simulation

Calculations of the forming limit strain and forming limit diagrams (FLD) are performed using the procedure of Barata da Rocha and Jalinier [39]. The flow curve of dual-phase steel is chosen as

$$\sigma_e = [\sigma_0 + H \ln (\bar{\varepsilon} + \bar{\varepsilon}_0)]\dot{\bar{\varepsilon}}^m$$

where σ_e is the flow stress, $\bar{\varepsilon}$ the effective strain, $\dot{\bar{\varepsilon}}$ the effective strain rate and σ_0, H, $\bar{\varepsilon}_0$, m are constants. The defect due to damage F is introduced instead of the geometrical defect f. At each step of the straining the overall defect in the material will grow according to two phenomena [36]: (a) the increase of the necking due to non-uniform plasticity dF_p, and (b) the increase in defect due to internal damage growth dF. dF_p is calculated from the instability model and dF is obtained by differentiating Equations 5 and 6.

4.4. Results

The FLD of dual-phase steel is computed in the expansion range assuming that the rolling direction is perpendicular to the major principal stress axis. Three damage conditions have been examined (Fig. 18):

(a) it is assumed that the overall volume fraction of voids is the same as in the real material but evenly distributed;

(b) the FLD is determined in one area in which the void volume fraction is maximum; and

(c) the FLD is determined in one area of

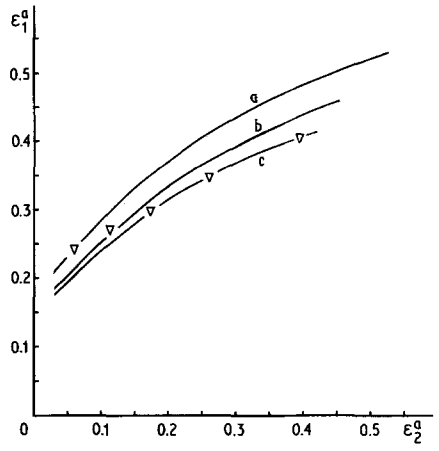

Figure 18 Forming limit diagram for the dual-phase steel under linear strain in the expansion range: (a) with a uniform void distribution; (b) with a non-uniform void distribution (on the basis of the observations); (c) with a non-uniform void distribution superimposed on a cavity band. ▽, experimental points. ε_1^a and ε_2^a are the principal strains in the plane of the sheet.

maximum void volume fraction and which contains a cavity band.

Curve (c) in Fig. 18, which reflects the real state of the material, is in good agreement with the experimental points. This result is the more interesting as it is obtained without the use of fitting parameters. Moreover, it is shown that if the cavities were evenly distributed (Curve (a)), the sheet formability would increase by about 20%.

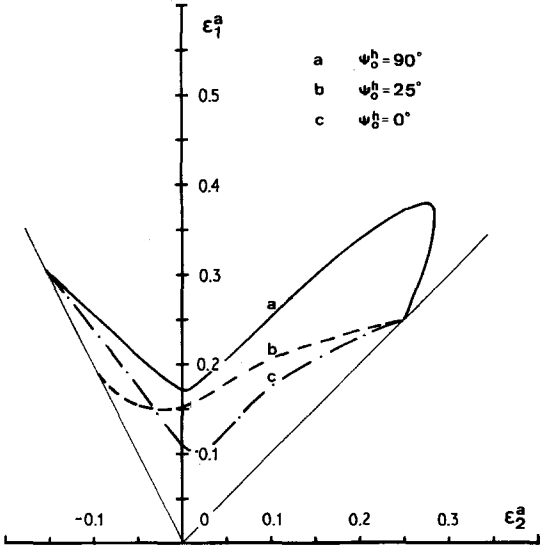

Figure 19 Forming limit diagrams for the dual-phase steel based on a statistical defect due to internal damage or a groove in the rolling direction (ψ_0^h is the inital angle between the groove and the direction of the minor principal stress).

On a given strain path, the forming limit is obtained for the groove orientation (ψ) which leads to the minimum calculated limit strain [39]. In the case of an isotropic material the FLD does not depend on the blank orientation. When dual-phase steel is strained along a given strain path, necking can occur in two directions if these are not superimposed: (a) the most mechanically favourable direction where the statistical defect develops, and (b) the direction of the structural defect (rolling).

In the second case, although the direction of the structural defect is less favourable, necking can occur since the resulting defect factor $F = 1 - D$ is larger than the statistical defect factor. Assuming the structural defect to be due to a cavity band, the FLD of the dual-phase steel is computed for two orientations of the rolling: (a) rolling perpendicular to the major principal axis, and (b) rolling parallel to the minor principal axis.

The two FLDs are not superimposed and the maximum difference between these two curves reaches 5%. In order to emphasize this anisotropic phenomenon, a larger structural defect, which corresponds to a groove of 20 μm depth for 0.7 mm sheet thickness is introduced in the computations. The initial angle between the groove and the minor principal stress axis is called ψ_0^h. During straining plastic flow can occur in two directions as mentioned before. As Fig. 19 illustrates, the FLDs are very sensitive to the groove orientation. In the case of dual-phase steel, the structural defect considered seems excessive, but for some other materials, the defect is realistic being generated by the interaction of cavity bands, elongated colonies of inclusions or grains with similar crystallographic orientations and roughnesses.

The necking direction can be predicted by this analysis. For anisotropic materials, some theoretical [44, 45] and experimental [46, 47] work shows that the critical limit strains are achieved for an initial groove orientation inclined at an angle $\psi \neq 0$. In the case of anisotropic materials subject to linear strain, the critical groove orientation corresponds to an angle $\psi = 0$ in the whole expansion range. However, in this work, preferred necking orientations ($\psi \neq 0$) can be predicted for isotropic materials.

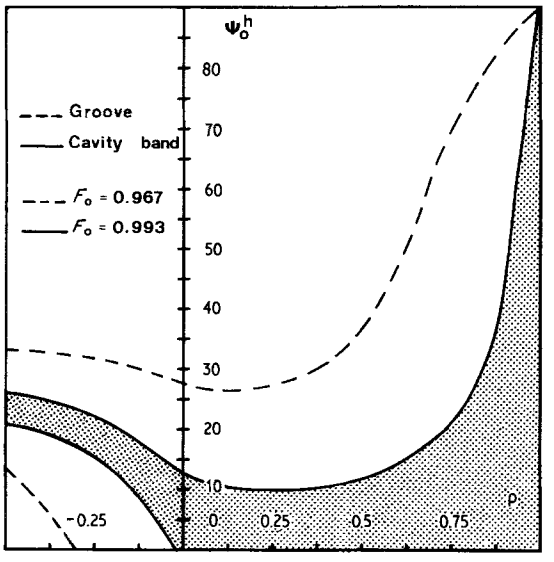

Figure 20 Conditions required to initiate necking in the direction of the cavity band (in grey) or in the direction of the groove (between the dashed lines).

Under a given linear strain path, for instance $\varrho = 0.75$, necking occurs on the statistical defect ($\psi = 0$) or on the structural defect ψ^h. If the structural defect is a cavity band, it will impose a localized plastic flow for ψ_0^h values bounded by $\pm 20°$. Fig. 20 shows the conditions required for the structural defect to impose a localized plastic flow under any linear strain path.

5. Conclusions

(a) In the present work, emphasis is put on the heterogeneous nature of the void distribution in a dual-phase steel. Although this phenomenon gives experimental results which must be taken with care, it is important to account for it, since the scale of the heterogeneities is similar to the scale of necking.

(b) Two types of heterogeneity are observed: on the one hand, the sheet can be divided into areas in which the void volume fraction is roughly constant but differs from one area to another; on the other hand, the sheet contains some bands aligned in the rolling direction where the cavities are highly concentrated.

(c) The scattered relative density change measurements are explained by a model based on the heterogeneous distribution of inclusions and associated damage.

(d) A model of plastic instability for void-containing material is developed. This model is powerful since it takes the physical aspect of the damage into account. It leads to a prediction of the FLD in good agreement with experiment.

(e) It is shown that the heterogeneities decrease the formability of the sheet by about 20% in comparison with a material which would contain the same number of cavities but evenly distributed.

(f) Preferred orientations of the necking direction are due to the structural heterogeneities, and lead to anisotropic forming limit diagrams.

Acknowledgements

The authors want to express their thanks to the Sollac Company for providing the metal and to Mr G. Boutet for technical assistance in the density measurements.

Appendix A

Statistical defect calculation

A material is supposed to contain one class of equiaxed cavities modelled by a parallelepiped of dimensions D_1, D_2 and D_3 (Fig. 21). Fig. 17 is a section of the sheet thickness. Each cavity can occupy a position in one of the v slices of the material, where

$$v = t/D_3$$

The length L of each slice is determined by the cavity volume fraction of the material:

$$C_v = D_1/L$$

If one supposes that the cavities occupy discrete positions separated by the distance dh, then the probability that the slice of width dh will intercept one cavity is

$$p = \frac{(D_1/\mathrm{d}h)}{(L/\mathrm{d}h)} = C_v$$

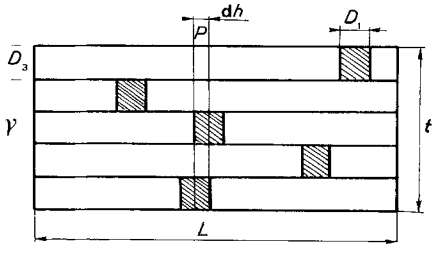

Figure 21 Model of the sheet thickness for one class of cavities.

The local defect D_p, corresponding to the alignment of x cavities along a line through Point P and normal to the sheet plane is expressed by

$$D_p = 1 - F_p = xD_3/t = x/v$$

The value of $D_p = 0$ or $F_p = 1$ corresponds to the case where there is no defect. The probability of finding such defect D_p is given by the binomial law:

$$p(x \text{ cavities}) = \binom{v}{x} C_v^x (1 - C_v)^{v-x}$$

Knowing this probability, it is then possible to represent a plane of the sheet (Fig. 14). The unshaded squares correspond to points without defects. The shaded squares represent points for which a line normal to the sheet plane and passing through them intercepts one or several cavities. The defect which leads to the necking will start at sections containing the maximum number of local defects. In order for the mechanical plastic instability model to apply, it will be assumed that the defect is quasi-linear. Also, in order for the band to be continuous, this must pass through squares without defects.

Various representations identical to that of Fig. 14 have been simulated by varying the probability p of the existence of a point defect at Point P of the sheet. The probability p^h of finding a defect in the quasi-linear band is calculated as a function of p:

$$p^h = -4p^2 + 4p \quad \text{if } 0 < p < 0.5$$

$$p^h = 1 \quad \text{if } 0.5 < p < 1$$

The linear defect F can be defined as the sum of the average of the local defects affected by the probability p^h and of 1 (points without defect) affected by the probability $1 - p^h$:

$$F = \left(\frac{\sum_1^v p(x = k)\,(1 - k/v)}{\sum_1^v p(x = k)} \right) p^h + (1 - p^h)$$

After a long but straightforward calculation, we obtain

$$F = \left[1 - \frac{C_v}{1 - (1 - C_v)^v} \right] p^h + 1 - p^h$$

This calculation process is the same for two classes of cavities.

Appendix B

Structural defect calculation

A section perpendicular to the sheet plane is supposed to contain a cavity band with two classes of voids regularly aligned in the rolling direction, and at an angle ψ to the minor principal axis (Fig. 22). The defect associated with the instability process is

$$F = 1 - D = S/(t\, l_\psi)$$

where S is the effective area and l_ψ the spacing between two voids. Using the void growth laws,

$$dR_i/R_i = C\, d\varepsilon_i - K\, d\varepsilon_3$$

and it follows that

$$F = 1 - (R_\psi^A R_{0A_0} + R_\psi^B R_{0B_0})/2\, t_0 l_\psi$$

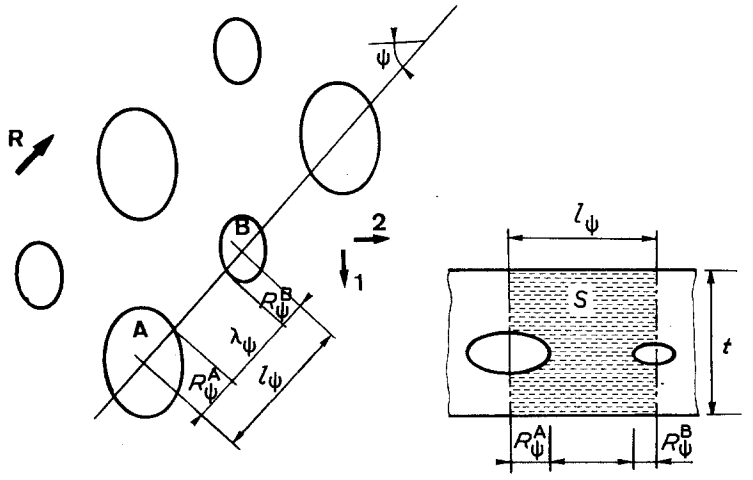

Figure 22 Defect induced by a cavity band. R is the rolling direction.

with

$$R_\psi = R_2^2 \cos^2\psi + R_1^2 \cos^2\psi$$

$$l_\psi = l_0 \exp \varepsilon_1 \{\sin^2\psi_0 + \cos^2\psi_0 \times \exp [2\varepsilon_1(\varrho - 1)]\}^{1/2}$$

References

1. J. M. JALINIER, J. H. SCHMITT, R. ARGEMI, J. L. SALSMANN and B. BAUDELET, *Mem. Sci. Rev. Met.* **3** (1980) 313.
2. J. LEMAITRE and J. L. CHABOCHE, *J. Mech. Appl.* **2** (3) (1978) 317.
3. R. T. RATCLIFFE, *Brit. J. Appl. Phys.* **16** (1965) 1193.
4. B. LETHINEN and A. MELANDER, *Metallography* **13** (1980) 283.
5. F. BARLAT, J. M. JALINIER and J. H. SCHMITT, *Mater. Tech.* in press.
6. M. C. SOUZA NOBREGA, B. FIDELIS DA SILVA, G. FERRAN, J. M. JALINIER and B. BAUDELET, *Mem. Sci. Rev. Met.* **3** (1980) 293.
7. R. T. DE HOFF and F. N. RHINES, "Microscopie quantitative" (Masson, Paris, 1972).
8. J. H. SCHMITT and J. M. JALINIER, *Acta Metall.* **30** (1982) 1789.
9. A. MELANDER, Proceedings of 12th Congress of the International Deep Drawing Research Group, S. Margherita Ligure, Italy, May 1982 (Associazone Italiano di Metallurgia) WG1 p. 17.
10. A. F. SZCEWCZYK and J. GURLAND, *Met. Trans.* **13A** (1982) 1821.
11. M. S. RASHID, "Formable HSLA and Dual Phase Steels", edited by A. T. Davenport (TMS–AIME, New York, 1979) p. 1.
12. R. A. JAGO and P. S. BABURAMANI, Proceedings of 4th RISO International Symposium on Metallurgy and Materials Sciences, Roskilde, Denmark, September 1983, p. 313.
13. J. H. SCHMITT, R. ARGEMI, J. M. JALINIER and B. BAUDELET, *J. Mater. Sci.* **16** (1981) 2004.
14. H. CLEEMOLA and U. BACKLUND, Proceedings of 12th Congress of the International Deep Drawing Research Group, S. Margherita Ligure, Italy, May 1982 (Associazone Italiano di Metallurgia) WG1 p. 49.
15. F. BARLAT, A. BARATA DA ROCHA and J. M. JALINIER, *J. Mater. Sci.* **19** (1984) 4133.
16. J. GURLAND and J. PLATEAU, *Trans. Amer. Soc. Metals* **56** (1963) 442.
17. D. BROEK, *Eng. Fract. Mech.* **5** (1973) 55.
18. K. TANAKA, T. MORI and T. NAKAMURA, *Phil. Mag.* **21** (1970) 267.
19. M. F. ASHBY, *ibid.* **14** (1966) 1157.
20. J. D. ARGON, J. IM and R. SAFOGLU, *Met. Trans.* **6A** (1975) 825.
21. L. M. BROWN and W. M. STOBBS, *Phil. Mag.* **34** (1976) 351.
22. S. H. GOODS and L. M. BROWN, *Acta Metall.* **27** (1979) 1.
23. F. M. BEREMIN, *Metall. Trans.* **12A** (1981) 723.
24. J. R. FISCHER and J. GURLAND, *Metal Sci.* **5** (1981) 193.
25. J. R. RICE and D. M. TRACEY, *J. Mech. Phys. Solids* **17** (1969) 201.
26. D. M. TRACEY, *Eng. Fract. Mech.* **3** (1971) 301.
27. A. MELANDER, *Mater. Sci. Eng.* **58** (1983) 63.
28. C. C. CHU, *Int. J. Solid Struct.* **16** (1980) 913.
29. A. L. GURSON, *J. Eng. Mater. Tech.* **99** (1977) 2.
30. J. M. JALINIER, DSc thesis, University of Metz (1981).
31. Z. MARCINIAK and K. KUCZYNSKI, *Int. J. Mech. Sci.* **9** (1967) 609.
32. Z. MARCINIAK, K. KUCZINSKI and T. POKORA, *ibid.* **15** (1973) 789.
33. A. NEEDLEMAN and N. TRIANTAFYLLIDIS, *J. Eng. Mater. Tech.* **100** (1978) 164.
34. C. C. CHU and A. NEEDLEMAN, *ibid.* **102** (1980) 249.
35. A. MELANDER and A. THUVANDER, *Scand. J. Metals* **12** (1983) 217.
36. J. M. JALINIER and J. H. SCHMITT, *Acta Metall.* **30** (1982) 1799.
37. H. VAN MINH, R. SOWERBY and J. L. DUNCAN, *Int. J. Mech. Sci.* **17** (1975) 339.
38. *Idem, ibid.* **16** (1974) 31.
39. A. BARATA DA ROCHA and J. M. JALINIER, *Trans. Iron Steel Inst. Jpn.* **24** (2) (1984) 132.
40. F. BARLAT, D.-Ing. thesis, Institut National Polytechnique, Grenoble (1984).
41. D. V. WILSON and O. ASCELRAD, Proceedings of 10th Congress of the International Deep Drawing Research Group, Warwick, England, April 1978, p. 155.
42. J. M. JALINIER, *J. Mater. Sci.* **18** (1983) 1794.
43. G. LE ROY, J. D. EMBURY, G. EDWARDS and M. F. ASHBY, *Acta Metall.* **29** (1981) 1509.
44. A. BARATA DA ROCHA, F. BARLAT and J. M. JALINIER, Proceedings of 13th Congress of the International Deep Drawing Research Group, Melbourne, Australia, February 1984.
45. *Idem, Mater. Sci. Eng.* **68** (1984/5) 151.
46. D. V. WILSON, W. T. ROBERTS and P. M. B. RODRIGUES, *Met. Trans.*, **12A** (1981) 1595.

Received 8 October
and accepted 6 November 1984